© 2017. Published by The Company of Biologists Ltd | Journal of Cell Science (2017) 130, 689-696 doi:10.1242/jcs.196139

SHORT REPORT

Tension regulates myosin dynamics during *Drosophila* embryonic wound repair

Anna B. Kobb[1,2], Teresa Zulueta-Coarasa[1,2] and Rodrigo Fernandez-Gonzalez[1,2,3,4,*]

ABSTRACT

Embryos repair epithelial wounds rapidly in a process driven by collective cell movements. Upon wounding, actin and the molecular motor non-muscle myosin II are redistributed in the cells adjacent to the wound, forming a supracellular purse string around the lesion. Purse string contraction coordinates cell movements and drives rapid wound closure. By using fluorescence recovery after photobleaching in *Drosophila* embryos, we found that myosin turns over as the purse string contracts. Myosin turnover at the purse string was slower than in other actomyosin networks that had a lower level of contractility. Mathematical modelling suggested that myosin assembly and disassembly rates were both reduced by tension at the wound edge. We used laser ablation to show that tension at the purse string increased as wound closure progressed, and that the increase in tension was associated with reduced myosin turnover. Reducing purse string tension by laser-mediated severing resulted in increased turnover and loss of myosin. Finally, myosin motor activity was necessary for its stabilization around the wound and for rapid wound closure. Our results indicate that mechanical forces regulate myosin dynamics during embryonic wound repair.

KEY WORDS: Cytoskeletal dynamics, Cell mechanics, Embryonic wound healing, *Drosophila*, Fluorescence recovery after photobleaching, Laser ablation

INTRODUCTION

Coordinated cell movements drive embryonic development and tissue repair, and are implicated in cancer metastasis (Gaggioli et al., 2007; Hidalgo-Carcedo et al., 2011). Cell movements are often coordinated by supracellular cytoskeletal networks formed by actin and the molecular motor non-muscle myosin II (Blankenship et al., 2006; Fernandez-Gonzalez et al., 2009; Lienkamp et al., 2012; Heller et al., 2014; Rozbicki et al., 2015).

Embryonic wound closure is a conserved process driven by the collective migration of cells to rapidly seal a lesion. During embryonic wound repair, actin and myosin are polarized in the cells adjacent to the wound, accumulating at the interface with the wounded cells and forming a supracellular cable around the wound (Martin and Lewis, 1992; Brock et al., 1996; Kiehart et al., 2000; Davidson et al., 2002; Kofron et al., 2002; Wood et al., 2002; Clark et al., 2009). The actomyosin cable contracts (Fernandez-Gonzalez and Zallen, 2013), serving as a purse string that coordinates the migratory behaviours of the cells adjacent to the wound (Brock et al., 1996; Wood et al., 2002; Abreu-Blanco et al., 2012). Embryonic wound closure can last minutes or hours, with total myosin levels at the purse string remaining relatively constant (Fernandez-Gonzalez and Zallen, 2013). The dwell times of myosin motors on actin filaments *in vitro* are of just a few seconds (Norstrom et al., 2010; Nagy et al., 2013; Hundt et al., 2016), suggesting that myosin motors may constantly turn over during wound closure. However, the mechanisms that regulate myosin dynamics in supracellular networks are not well understood.

Physical forces can regulate myosin dynamics both *in vitro* and *in vivo*. *In vitro*, non-muscle myosin II motors under mechanical load are stabilized on actin filaments (Kovacs et al., 2007). *In vivo*, mechanical tension controls the cortical localization of myosin in mitotic *Dictyostelium* cells (Effler et al., 2006), and in the ectoderm (Fernandez-Gonzalez et al., 2009) and mesoderm (Pouille et al., 2009) of early *Drosophila* embryos. It is currently unknown whether mechanical forces affect myosin dynamics during embryonic wound repair.

RESULTS AND DISCUSSION

Myosin turnover is reduced around embryonic wounds

We investigated myosin dynamics during the repair of laser-induced wounds in the epidermis of *Drosophila* embryos. Wound repair occurred in a fast phase followed by a slow phase (Fig. S1) (Abreu-Blanco et al., 2012). We conducted our measurements within the fast phase (unless otherwise indicated), when wound area was 40–60% of its maximum value.

We compared myosin dynamics in supracellular networks displaying different degrees of contractility, the purse string and actomyosin cables that segment the epidermis (Simone and DiNardo, 2010) (Movie 1). Myosin fluorescence correlates with tension (Fernandez-Gonzalez et al., 2009). In embryos expressing myosin regulatory light chain (MRLC, a subunit of myosin II motors; known as Sqh in flies) tagged with the green fluorescent protein (GFP), fluorescence at the purse string was 1.9-fold greater than in epidermal cables ($P<0.005$, Fig. 1C,D,F). Similar results were found for GFP-tagged myosin heavy chain (MHC, another myosin subunit; known as Zip in flies; Fig. S2A,B,D). We used ultraviolet laser ablation to quantify relative tension levels (Hutson et al., 2003; Zulueta-Coarasa and Fernandez-Gonzalez, 2015) (Fig. 1A,B). The retraction velocity after severing the purse string was 40% greater than that of epidermal cables ($P<0.02$, Fig. 1E, inset). Thus, assuming constant viscoelastic properties, our results indicate that tension is greater in wound-associated purse strings than in epidermal cables.

To investigate whether myosin turnover at the purse string is affected by contractile force, we used fluorescence recovery after

[1]Institute of Biomaterials and Biomedical Engineering, University of Toronto, Toronto, Ontario, Canada M5S 3G9. [2]Ted Rogers Centre for Heart Research, University of Toronto, Toronto, Ontario, Canada M5G 1M1. [3]Department of Cell and Systems Biology, University of Toronto, Toronto, Ontario, Canada M5S 3G5. [4]Developmental and Stem Cell Biology Program, The Hospital for Sick Children, Toronto, Ontario, Canada M5G 1X8.

*Author for correspondence (rodrigo.fernandez.gonzalez@utoronto.ca)

R.F.-G., 0000-0003-0770-744X

Received 4 August 2016; Accepted 3 January 2017

Journal of Cell Science (2017) 130, 689-696 doi:10.1242/jcs.196139

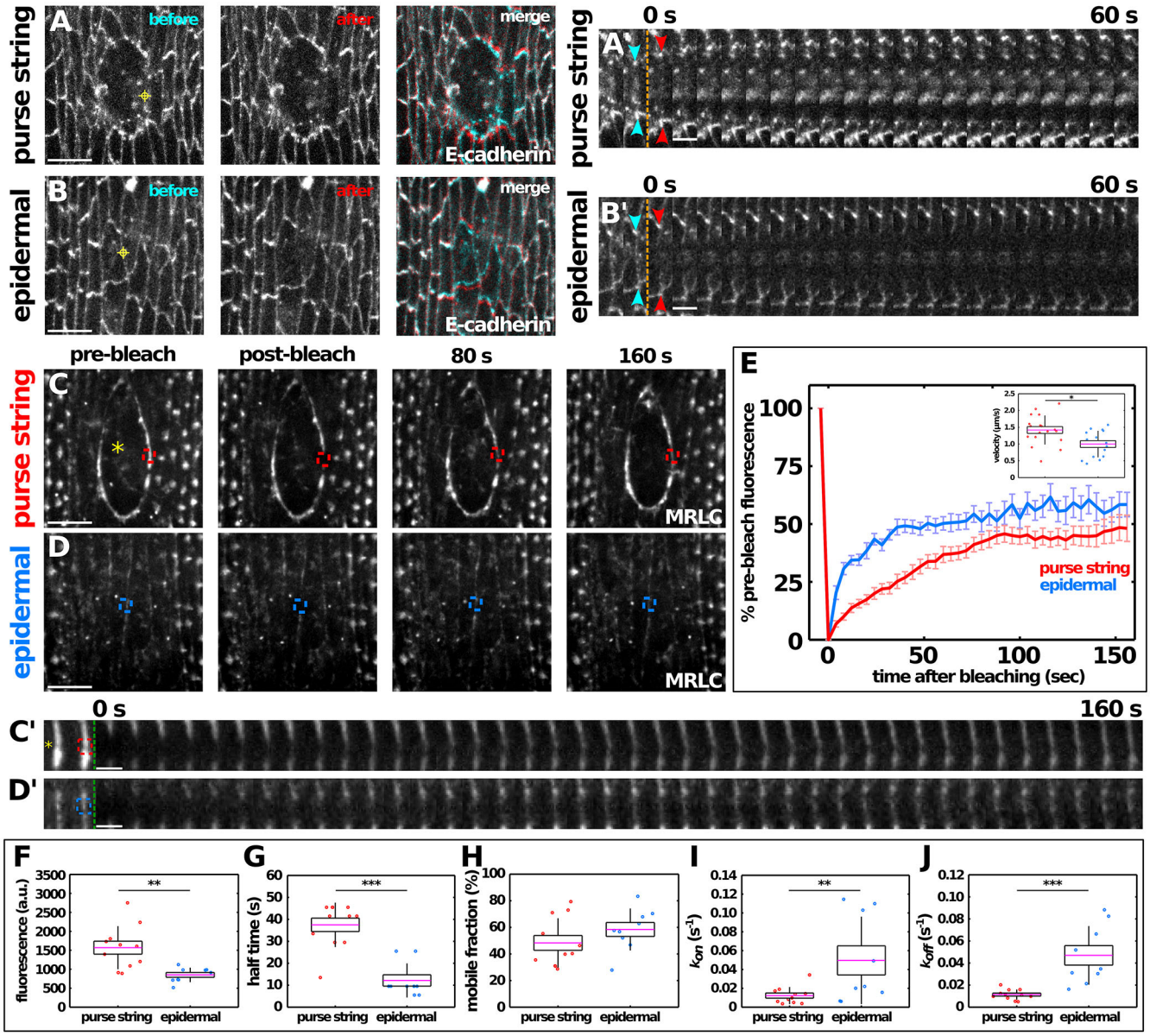

Fig. 1. MRLC turnover is reduced at the purse string. (A,B) Laser ablation of the wound margin (A) and an epidermal cable (B) in embryos expressing E-cadherin:mTomato. Cells immediately before (left, cyan in merge) and after (centre, red in merge) ablation. Yellow targets indicate ablation sites. (A′,B′) Kymographs showing recoil of the severed ends after ablation. Arrowheads indicate the position of the vertices delimiting the severed segment prior to (cyan) or immediately after (red) ablation. Orange dashed lines indicate the time of ablation. (C,D) FRAP experiments in wounded embryos expressing MRLC–GFP. Regions were photobleached on the purse string (C, red) or an epidermal cable (D, blue). Yellow asterisks indicate the position of the wound. (C′,D′) Kymographs of experiments in C and D. Green dashed lines show the time of photobleaching. In all images, anterior is left and ventral down. Scale bars: 10 µm (A–D), 3 s (A′,B′) and 4 s (C′,D′). (E–J) Percentage pre-bleach fluorescence over time (mean±s.e.m.) in the photobleached region (E), initial fluorescence (F), $t_{1/2}$ (G), mobile fraction (H), k_{on} (I) and k_{off} (J) for purse string (red, n=11) and epidermal cables (blue, n=9). The inset in E shows recoil velocity after laser ablation of the wound edge (red, n=18) or epidermal cables (blue, n=15). au, arbitrary units. For box plots, error bars show the s.d., the box indicates the s.e.m. and magenta lines denote the mean. *P<0.05; **P<0.01; ***P<0.001 (Mann-Whitney test).

photobleaching (FRAP) of MRLC–GFP (Fig. 1C,D). At the purse string, MRLC turned over with a characteristic half-time, $t_{1/2}$, of 37.5±3.0 s (mean±s.e.m.; Fig. 1E,G,H). In epidermal cables, MRLC displayed a $t_{1/2}$ of 12.2±2.6 s, which was significantly shorter than at the purse string (P<0.001, Fig. 1G). We found that MHC:GFP was also stabilized at the wound margin (Fig. S2C,E,F). Taken together, our data indicate that myosin motors are stabilized at the wound edge during embryonic wound repair.

To understand how myosin turns over at the wound edge, we developed a mathematical model to extract the rates of myosin assembly (k_{on}) and disassembly (k_{off}) in the photobleached regions (Pines et al., 2012). Using the model, we estimated the assembly rate constant at the purse string to be 0.012±0.003 s^{-1}, significantly lower than the 0.050±0.015 s^{-1} in epidermal cables (P<0.01, Fig. 1I). The disassembly rate constant was also significantly lower at the purse string (0.011±0.001 s^{-1}) than in epidermal cables (0.047±0.009 s^{-1}, P<0.001, Fig. 1J). Taken together, our data indicate that the turnover of myosin is reduced at the wound edge, suggesting a role for tension in regulating myosin dynamics during wound closure.

Journal of Cell Science (2017) 130, 689-696 doi:10.1242/jcs.196139

Mechanical tension is necessary to stabilize myosin at the purse string

To determine whether physical forces affect myosin dynamics around the wound, we used laser ablation to sever the purse string, thereby partially releasing the tension that it sustained. We cut the purse string 10 min after wounding in embryos expressing MRLC–GFP, and we monitored fluorescence immediately after cutting in regions adjacent to the severed area (Fig. 2A), in regions that were far away (at least 30 µm, Fig. 2B) from the severed area, and in sham-irradiated controls (Fig. 2C). We measured a significant loss of 19.8±6.3% (mean±s.e.m.) of MRLC–GFP fluorescence in regions of the purse string adjacent to the severed area (15 out of 18 regions, $P<0.02$, Fig. 2D,D′). In contrast, MRLC–GFP fluorescence did not change in segments away from the ablation site or in controls (Fig. 2D,D′). These data indicate that tension is, at least in part, necessary to maintain myosin at the purse string around embryonic wounds.

To determine how loss of tension affects myosin dynamics at the purse string, we used FRAP to measure myosin turnover at ∼1 min after cutting the purse string in segments adjacent to or far from ablation sites, and in sham-irradiated controls (Fig. 2E,G; Movie 2). Myosin turnover was significantly faster close to the site of ablation than in controls ($t_{1/2}$ of 19.5±2.7 s vs 30.2±2.5 s, respectively, $P<0.01$, Fig. 2H). Our results indicate that tension is necessary to stabilize myosin and maintain it at the wound edge.

Mechanical tension is sufficient to stabilize myosin at the wound edge

To investigate whether tension is sufficient to stabilize myosin, we sought scenarios in which tension at the purse string increased. Using laser ablation, we found that the retraction velocity after severing the cable was 31.7% greater in the slow phase of wound closure (25 min after wounding, <10% of the maximum wound area) than in the fast phase (5 min after wounding, 40–60% of the maximum wound area, $P<0.01$, Fig. 3A,B,E, inset). Thus, tension at the purse string increased as the wound closed.

To determine the effect of increased tension on myosin dynamics, we compared MRLC–GFP turnover during the fast and slow phases of wound repair (Fig. 3C,D). Each purse string was photobleached during both the fast and slow phases. The $t_{1/2}$ of MRLC–GFP at the wound margin during the slow phase was 50.0±3.4 s, significantly longer than the 34.5±5.5 s in the fast phase (mean±s.e.m.; $P<0.02$, Fig. 3E–G). Using our mathematical model, we found that the k_{on} did not display significant changes (Fig. 3H), but the rate of myosin disassembly from the purse string, k_{off}, showed a significant decrease of 2-fold in the slow phase compared to the fast phase ($P<0.02$, Fig. 3I). Sequential photobleaching of epidermal cables did not cause any differences in the turnover of MRLC–GFP (Fig. S3). Taken together, our data show that increased tension is sufficient to stabilize myosin at the purse string, possibly through a decreased rate of myosin disassembly.

Motor activity is necessary for myosin stabilization and rapid wound closure

Phosphorylation of the MRLC at a serine and a threonine residue is necessary for myosin motor activity (Sellers et al., 1985; Jordan and Karess, 1997; Komatsu et al., 2000), minifilament formation (Scholey et al., 1980), and, to a lesser extent, efficient actin binding (Sellers et al., 1982). We investigated the role of phosphorylation on the stabilization of myosin at the wound border and tissue repair. We used embryos expressing GFP-tagged phosphomimetic (Sqh-AE, threonine-20 is mutated into an alanine and serine-21 is mutated into a glutamic acid), unphosphorylatable (Sqh-AA) or wild-type (Sqh-TS) forms of the MRLC (Vasquez et al., 2014) (Fig. 4A–E). Recent data indicate that Sqh-AE may not fully mimic the phosphorylated state of myosin, but rather displays partially defective motor activity (Vasquez et al, 2016). Endogenous myosin activity was depleted by injection of the Rho kinase (Rok) inhibitor Y-27632 (Fernandez-Gonzalez et al., 2009) in embryos expressing the phosphorylation mutant MRLC variants. Y-27632 treatment at 8–10 min after wounding led to a 46.0±3.2% loss of wild-type myosin from the wound edge within 1 min, a greater percentage than the 25.8±4.3% loss of Sqh-AA, and the 8.5±4.7% loss of Sqh-AE (mean±s.e.m.; $P<0.01$; Fig. S4, Movie 3). Our data suggest that cortical localization of phosphorylation mutant myosin only partially requires Rok activity.

Stabilization at the wound edge was disrupted for Sqh-AA and Sqh-AE (Fig. 4F). Upon endogenous myosin deactivation, both Sqh-AA ($t_{1/2}$ of 15.7±3.1 s) and Sqh-AE (21.2±3.2 s) turned over faster than wild-type myosin (36.7±3.7 s; $P<0.01$ and $P<0.05$, respectively; Fig. 4F′). Sqh-AE was stabilized (51.8±4.2 s) in the presence of endogenous myosin ($P<0.01$). In contrast, the turnover of Sqh-AA, which cannot form minifilaments with other motors (Scholey et al., 1980), was not affected by the presence of endogenous myosin (18.1 ±3.2 s). Our data suggest that motor activity and the ability to form minifilaments are crucial for myosin II motors to be stabilized in the purse string during embryonic wound repair.

To establish the role of myosin stabilization during embryonic repair, we measured wound closure dynamics in embryos expressing wild-type or phosphorylation mutant myosin (Fig. 4I–N). In embryos in which endogenous myosin was active, wounds closed independently of the expression of phosphorylation mutant myosin (Fig. 4I–K,N). In contrast, in embryos expressing the phosphorylation mutant constructs and where endogenous myosin activity was inhibited by injection of Y-27632 after the purse string had formed and wound closure had begun, wounds did not close, but rather expanded again (Fig. 4L–N). Taken together, these results suggest that motor activity facilitates myosin stabilization at the wound edge and promotes rapid wound closure.

Our results indicate that myosin is mechanically regulated during the collective cell movements that drive embryonic wound repair. We find that dynamic motor activity is crucial for the stabilization of myosin at the cortex, consistent with recent work showing that myosin phosphorylation regulates contractility in epithelial morphogenesis (Kasza et al., 2014; Vasquez et al., 2014; Vasquez et al., 2016). Several actin regulators are sensitive to load, including formins (Courtemanche et al., 2013; Higashida et al., 2013; Jégou et al., 2013), and the filament-severing protein cofilin (Hayakawa et al., 2011; Tojkander et al., 2015). The mechanical dependence of myosin dynamics could thus be a result of direct effects on the motor, indirect effects on the actin filaments bound by the motor, or a combination of both. Changes to the physical properties at the wound edge may also locally affect the dynamics of myosin and actin during wound repair. Recent advances in genome editing and the development of new methods to probe tissue mechanics in living animals (Campàs et al., 2014; Bambardekar et al., 2015) will be of enormous value to investigate the interplay between cell mechanics and myosin dynamics during collective cell migration *in vivo*.

MATERIALS AND METHODS

Fly stocks

Live imaging was conducted using *sqh-sqh:GFP* (*sqh* encodes MRLC, and here *sqh* is expressed under its own promoter) (Royou et al., 2004), *sqh-sqh^{TS}:GFP*, *sqh-sqh^{AE}:GFP*, and *sqh-sqh^{AA}:GFP* (Vasquez et al., 2014), *zip-zip:*

Journal of Cell Science (2017) 130, 689-696 doi:10.1242/jcs.196139

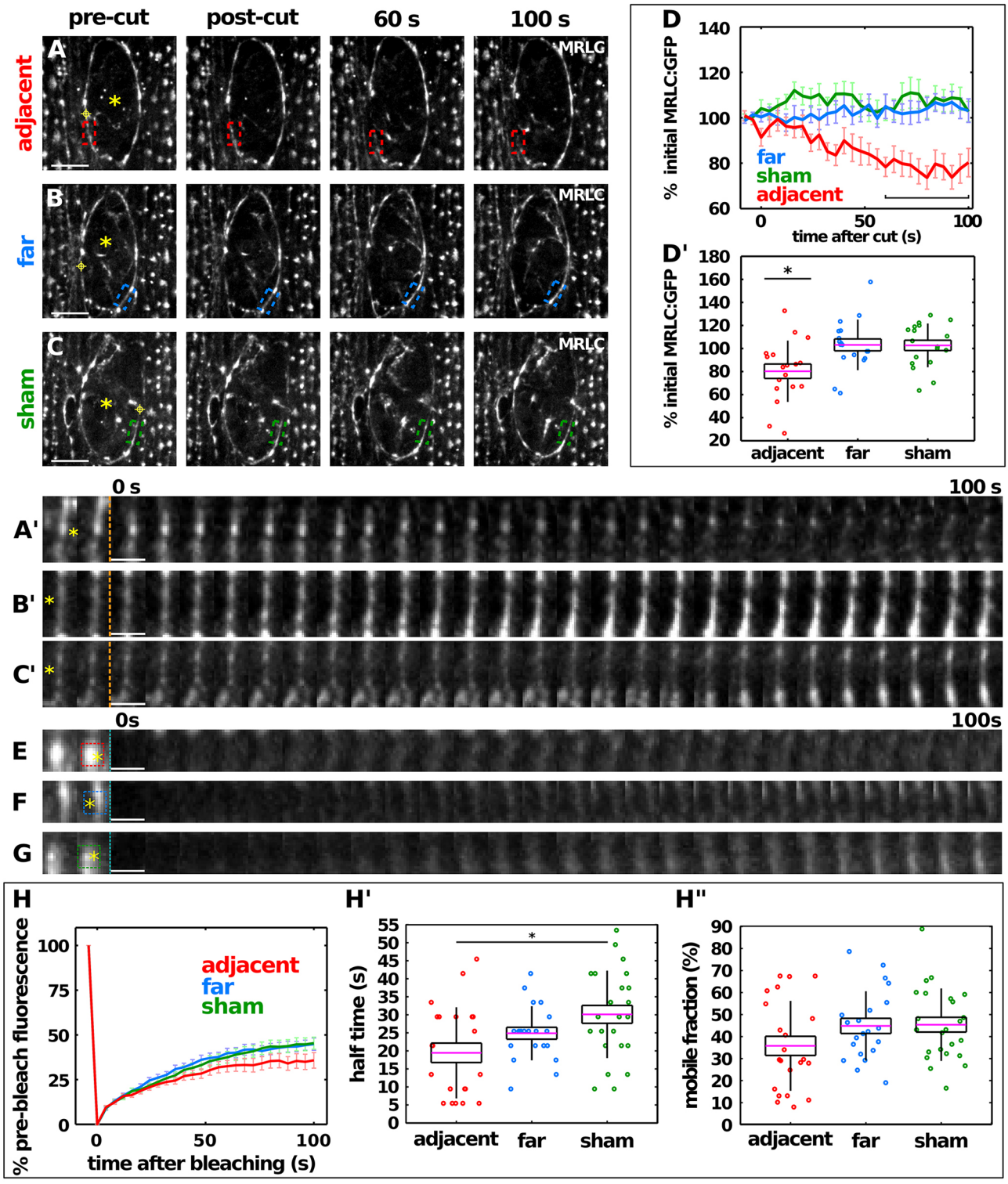

Fig. 2. Tension is necessary to stabilize and maintain myosin at the wound margin. (A–C) Wounded embryos expressing MRLC–GFP and irradiated with ultraviolet light (A,B) or sham (C) irradiated. Yellow targets indicate ablation sites. Boxes show the region where fluorescence was monitored, adjacent (A) or far (B) from the ablation site, or in sham-irradiated controls (C). (A′–C′) Kymographs of experiments in A–C. Orange dashed lines indicate the time of irradiation. Scale bars: 10 µm (A–C); 4 s (A′–C′). (D) Mean±s.e.m. MRLC–GFP fluorescence normalized to the fluorescence before severing the purse string (D), and percentage change in MRLC–GFP fluorescence 100 s after severing the purse string (D′), for regions adjacent to the site of ablation (n=18), far from the site (n=9) or in sham-irradiated purse strings (n=9). The black bracket in D indicates stabilization of myosin fluorescence in regions adjacent to the ablation site 1 min after ablation. (E–G) Kymographs of MRLC–GFP FRAP in purse string segments adjacent to the ablation site (E, red), far (F, blue), or in sham-irradiated controls (G, green). Cyan dashed lines indicate the time of photobleaching. Scale bars: 4 s. Yellow asterisks indicate the position of the wound. In all images, anterior is left and ventral down. (H) Percentage pre-bleach fluorescence over time (mean±s.e.m.) in the photobleached region (H), $t_{1/2}$ (H′), and mobile fraction (H″) for regions adjacent (red, n=22) or far (blue, n=20) from the ablation site, and in sham-irradiated controls (green, n=24). For box plots, error bars show the s.d., the box indicates the s.e.m. and magenta lines denote the mean. *P<0.05 (Dunn's test).

Journal of Cell Science (2017) 130, 689-696 doi:10.1242/jcs.196139

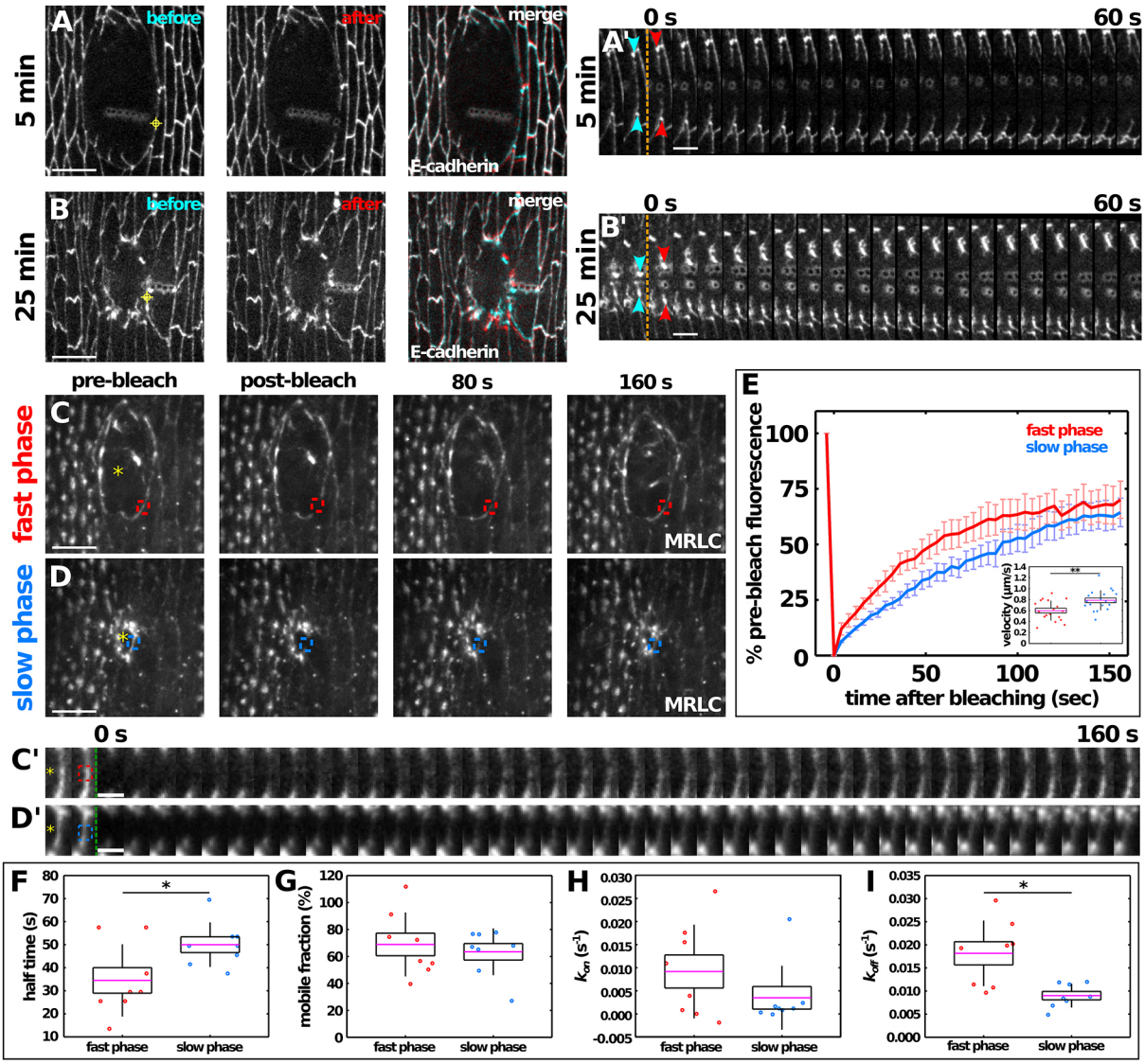

Fig. 3. Tension is sufficient to stabilize myosin at the purse string. (A,B) Laser ablation of segments of the wound margin 5 min (A) and 25 min (B) after wounding in embryos expressing E-cadherin:GFP. Images are immediately before (left, cyan in merge) and after (centre, red in merge) ablation. Yellow targets indicate ablation sites. (A′,B′) Kymographs showing recoil of the severed ends after ablation. Arrowheads indicate the position of the vertices delimiting the severed junction prior to (cyan) or immediately after (red) ablation. Orange dashed lines indicate the time of ablation. (C,D) FRAP experiments in wounded embryos expressing MRLC–GFP. Regions on the purse string were photobleached during the fast phase (C, red) or the slow phase of wound closure (D, blue). (C′,D′) Kymographs of experiments in C and D. Green dashed lines show time of photobleaching. Yellow asterisks indicate the position of the wound. In all images, anterior is left and ventral down. Scale bars: 10 µm (A–D), 3 s (A′,B′), 4 s (C′,D′). (E–I) Percentage pre-bleach fluorescence over time (mean±s.e.m.) in the photobleached region (E), $t_{1/2}$ (F), mobile fraction (G), k_{on} (H) and k_{off} (I) for the fast phase (red, n=8) and the slow phase (blue, n=8). The inset in E shows recoil velocity after laser ablation of the wound edge 5 min (n=18) or 25 min (n=19) after wounding. For box plots, error bars show the s.d., the box indicates the s.e.m. and magenta lines denote the mean. *P<0.05; **P<0.01 (Mann–Whitney test in E, Wilcoxon signed-rank test in F-I).

GFP (*zip* encodes for MHC, here expressed under its own promoter) (Buszczak et al., 2007) and *endo-DE-cadherin:mTomato* (Huang et al., 2009).

Time-lapse imaging

Embryos at stage 14–15 of development were dechorionated in 50% bleach for 2 min and rinsed with water. Embryos were aligned on an apple juice–agar pad, glued ventrolateral-side-down onto a coverslip using heptane glue, and covered with a 1:1 mix of halocarbon oil 27 and halocarbon oil 700 (Sigma-Aldrich). Embryos were imaged using a Revolution XD spinning disk confocal (Andor) with a 60× oil-immersion lens (NA 1.35; Olympus). Images were captured with an iXon Ultra 897 camera (Andor) and Metamorph (Molecular Devices) as the image acquisition software. 16-bit *Z*-stacks were acquired at 0.2–0.3 µm steps every 4–30 s (7–16 slices per stack). Maximum intensity projections were used for analysis. In Fig. 4A–E, the contrast of the images was adjusted independently for each treatment. In all other figures, the same linear contrast adjustment was applied to all the images in each experiment.

Injections

Embryos were dechorionated and aligned as above, dehydrated for 10–15 min and covered in a 1:1 mix of halocarbon oil 27 and halocarbon oil 700. Embryos were injected with water or 100 mM Y-27632 (Tocris Biosciences) in water using a Transferman NK2 micromanipulator (Eppendorf) and a PV820 microinjector (WPI) coupled to our spinning disk confocal.

Laser ablation

Wounds were created using a pulsed Micropoint N_2 laser (Andor) tuned to 365 nm. The laser produced 120 µJ pulses with a duration of 2–6 ns. To wound embryos, ten laser pulses were delivered at each of seven spots over a

Journal of Cell Science (2017) 130, 689-696 doi:10.1242/jcs.196139

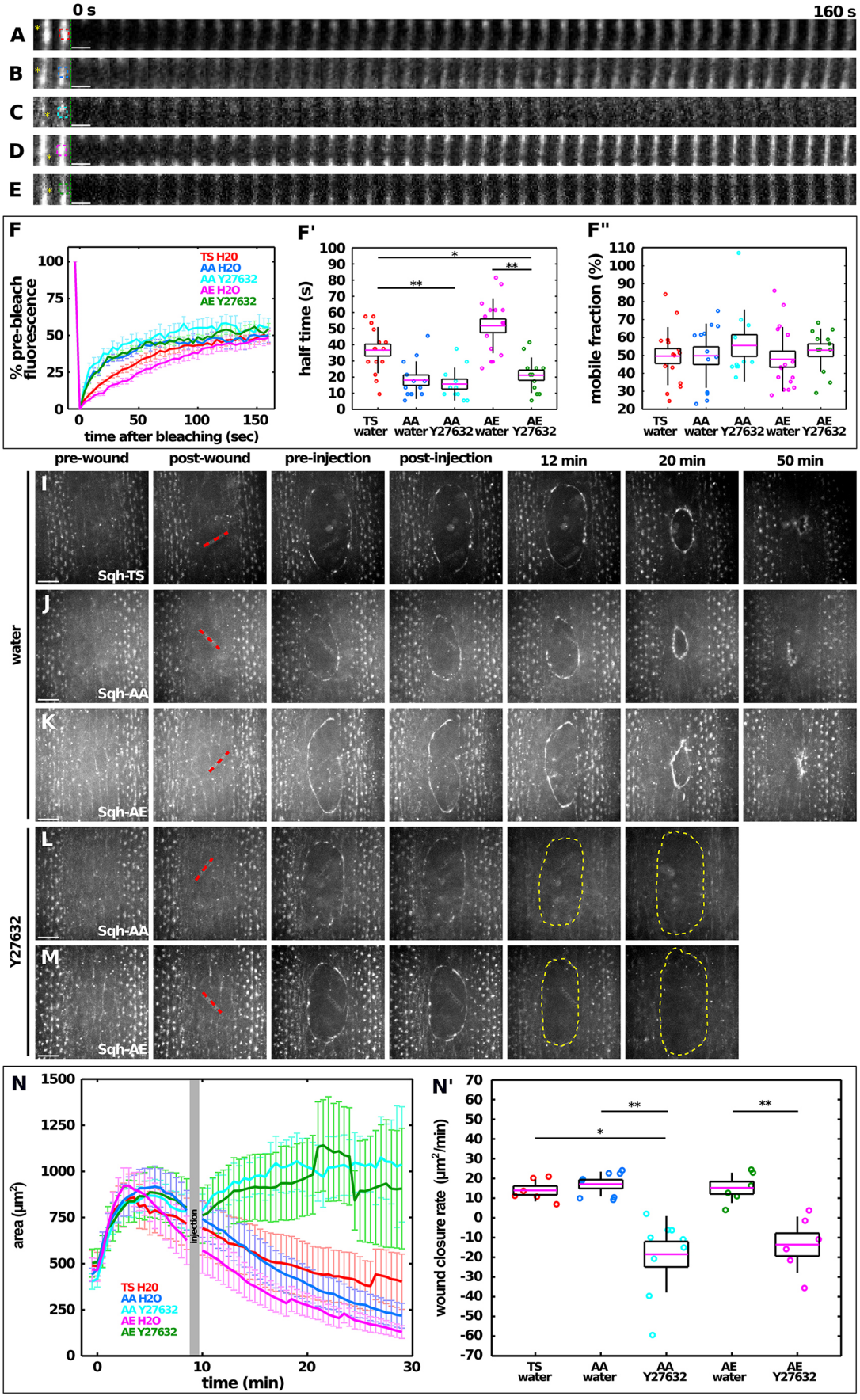

Fig. 4. See next page for legend.

Fig. 4. Phosphorylation flux is necessary for tension-mediated myosin stabilization. (A–E) Kymographs of purse string FRAP in embryos expressing Sqh-TS and injected with water (A, red), Sqh-AA and water-injected (B, blue), Sqh-AA and Y-27632-injected (C, cyan), Sqh-AE and water-injected (D, magenta), Sqh-AE and Y-27632-injected (E, green). Green dashed lines indicate time of photobleaching. Scale bars: 4 s. Yellow asterisks indicate the position of the wound. (F) Percentage pre-bleach fluorescence over time (mean ±s.e.m.) in the photobleached region (F), $t_{1/2}$ (F′), and mobile fraction (F″). Sqh-TS water-injected (n=15), Sqh-AA water-injected (n=13), Sqh-AA Y-27632-injected (n=11), Sqh-AE water-injected (n=16), Sqh-AE Y-27632-injected (n=12). (I–M) Wounded embryos expressing GFP-tagged wild-type (I), unphosphorylatable (J, L) or phosphomimetic myosin (K,M), injected with water (I–K) or Y-27632 (L–M). Times are with respect to wounding. Red lines indicate wound sites. Yellow dashed lines outline the wound. Scale bars: 10 µm. (N, N′) Wound area over time (mean±s.e.m., N) and wound closure rate (N′). Sqh-TS water-injected (n=6), Sqh-AA water-injected (n=8), Sqh-AA Y-27632-injected (n=9), Sqh-AE water-injected (n=9), Sqh-AE Y-27632-injected (n=6). In all images, anterior is left and ventral down. For box plots, error bars show the s.d., the box indicates the s.e.m. and magenta lines denote the mean. *P<0.05; **P<0.01 (Dunn's test).

14 µm line. To reduce or measure tension, ten laser pulses were delivered at a single spot, and samples were imaged immediately before and 1.72 s after spot ablation. In sham-irradiated controls, we completely attenuated the laser using a neutral density filter.

Image analysis

To track repair dynamics, wounds were delineated by using Livewire, a semi-automated optimal path search method for image segmentation integrated into SIESTA, an image analysis platform that we develop (Fernandez-Gonzalez and Zallen, 2011; Leung and Fernandez-Gonzalez, 2015). The wound closure rate was the area difference between the time after injection and the last time point of each movie, divided by the elapsed time. To measure recoil velocity after laser ablation, the positions of the tricellular vertices connected by the ablated cytoskeletal networks were manually tracked in SIESTA, and the velocity of retraction was calculated.

Fluorescence recovery after photobleaching

Photobleaching experiments were conducted by using the FRAPPA system (Andor) and a 488 nm laser. 10×10 pixel regions were photobleached using a dwell time of 500 µs/pixel. Two Z-stacks were acquired at 4 s apart prior to photobleaching. Photobleached regions were imaged every 4 s for 2–4 min. The fluorescence intensity in the photobleached region at time t, $f(t)$, was measured as:

$$f(t) = 100 \times \frac{[I_{ROI}(t) - I_{bg}(t)] - [I_{ROI}(0) - I_{bg}(0)]}{[I_{ROI}(before) - I_{bg}(before)] - [I_{ROI}(0) - I_{bg}(0)]} \times \frac{I_M(before) - I_{bg}(before)}{I_M(t) - I_{bg}(t)}, \quad (1)$$

where t=$before$ is the time immediately before photobleaching, t=0 is the time immediately after photobleaching, I_{ROI} is the mean pixel value within the photobleached region, I_{bg} is the background signal, calculated as the mean pixel value within a 10×10 pixel region outside the embryo, and I_M is the mean image intensity. The mobile fraction was the mean $f(t)$ value for the last two time points measured, and the half time ($t_{1/2}$) was the time required to reach half of the mobile fraction.

Mathematical modelling of FRAP

We modelled FRAP using a two-state model (Pines et al., 2012) to describe the association and dissociation of myosin to and from the purse string, with rate constants k_{on} and k_{off}, respectively:

$$I_U \underset{k_{off}}{\overset{k_{on}}{\rightleftarrows}} I_B, \quad (2)$$

where I_B and I_U represent the bound and unbound pools of fluorescent myosin, respectively. Briefly, fluorescence in the region of interest, $f(t)$, can be written as:

$$f(t) = \frac{k_{off}}{(k_{off} + k_{on})}[1 - e^{-t(k_{off}+k_{on})}], \quad (3)$$

or

$$f(t) = f_{max}[1 - e^{\frac{-t}{\tau}}], \quad (4)$$

where f_{max} is the mobile fraction, and τ is a characteristic time scale:

$$f_{max} = \frac{k_{off}}{k_{off} + k_{on}}, \quad (5)$$

$$\tau = \frac{1}{k_{off} + k_{on}}. \quad (6)$$

We fitted the FRAP data with (Eqn 4) and quantified f_{max} and τ using (Eqns 5 and 6):

$$k_{on} = \frac{1 - f_{max}}{\tau}, \quad (7)$$

$$k_{off} = \frac{f_{max}}{\tau}. \quad (8)$$

Statistical analysis

We compared sample means using a non-parametric Mann–Whitney test (Glantz, 2002). For comparisons of more than two groups, we used a Kruskal–Wallis test to reject the null hypothesis, and Dunn's test for pairwise comparisons. Sequential FRAP experiments were contrasted using Wilcoxon signed-rank test. For time series, error bars indicate s.e.m. For box plots, error bars show standard deviation, the box indicates the s.e.m. and magenta lines denote the mean. *P<0.05; **P<0.01; ***P<0.001.

Acknowledgements

We are grateful to Adam Martin for reagents; to Sérgio Simoes, Tony Harris, Jon Rocheleau, Will Ryu, and Jen Zallen for useful discussions; and to Miranda Hunter, Jessica Yu and Michael Wang for comments on the manuscript. Flybase provided important information for this work.

Competing interests

The authors declare no competing or financial interests.

Author contributions

A.B.K. and R.F.-G. conceived the study, designed the experiments, analysed the results and wrote the manuscript. A.B.K. and T.Z.-C. conducted the experiments.

Funding

This research was supported by the Ontario Ministry of Economic Development and Innovation (ER14-10-170 to R.F.-G., and Trillium Scholarship to T.Z.-C.), the Natural Sciences and Engineering Research Council of Canada (418438-13), the Canada Foundation for Innovation (30279), the Delta Kappa Gamma Society International (World Fellowship to T.Z.-C.), and University of Toronto, Institute of Biomaterials and Biomedical Engineering Wildcat and International Scholarships (to A.B.K.).

Supplementary information

Supplementary information available online at
http://jcs.biologists.org/lookup/doi/10.1242/jcs.196139.supplemental

References

Abreu-Blanco, M. T., Verboon, J. M., Liu, R., Watts, J. J. and Parkhurst, S. M. (2012). Drosophila embryos close epithelial wounds using a combination of cellular protrusions and an actomyosin purse string. *J. Cell Sci.* **125**, 5984-5997.

Bambardekar, K., Clément, R., Blanc, O., Chardès, C. and Lenne, P.-F. (2015). Direct laser manipulation reveals the mechanics of cell contacts in vivo. *Proc. Natl. Acad. Sci. USA* **112**, 1416-1421.

Blankenship, J. T., Backovic, S. T., Sanny, J. S. P., Weitz, O. and Zallen, J. A. (2006). Multicellular rosette formation links planar cell polarity to tissue morphogenesis. *Dev. Cell* **11**, 459-470.

Brock, J., Midwinter, K., Lewis, J. and Martin, P. (1996). Healing of incisional wounds in the embryonic chick wing bud: characterization of the actin purse-string and demonstration of a requirement for Rho activation. *J. Cell Biol.* **135**, 1097-1107.

Buszczak, M., Paterno, S., Lighthouse, D., Bachman, J., Planck, J., Owen, S., Skora, A. D., Nystul, T. G., Ohlstein, B., Allen, A. et al. (2007). The Carnegie protein trap library: a versatile tool for *Drosophila* developmental studies. *Genetics* **175**, 1505-1531.

Campàs, O., Mammoto, T., Hasso, S., Sperling, R. A., O'Connell, D., Bischof, A. G., Maas, R., Weitz, D. A., Mahadevan, L. and Ingber, D. E. (2014). Quantifying cell-generated mechanical forces within living embryonic tissues. *Nat. Methods* **11**, 183-189.

Clark, A. G., Miller, A. L., Vaughan, E., Yu, H.-Y. E., Penkert, R. and Bement, W. M. (2009). Integration of single and multicellular wound responses. *Curr. Biol.* **19**, 1389-1395.

Courtemanche, N., Lee, J. Y., Pollard, T. D. and Greene, E. C. (2013). Tension modulates actin filament polymerization mediated by formin and profilin. *Proc. Natl. Acad. Sci. USA* **110**, 9752-9757.

Davidson, L. A., Ezin, A. M. and Keller, R. (2002). Embryonic wound healing by apical contraction and ingression in Xenopus laevis. *Cell Motil. Cytoskeleton* **53**, 163-176.

Effler, J. C., Kee, Y.-S., Berk, J. M., Tran, M. N., Iglesias, P. A. and Robinson, D. N. (2006). Mitosis-specific mechanosensing and contractile-protein redistribution control cell shape. *Curr. Biol.* **16**, 1962-1967.

Fernandez-Gonzalez, R. and Zallen, J. A. (2011). Oscillatory behaviors and hierarchical assembly of contractile structures in intercalating cells. *Phys. Biol.* **8**, 045005.

Fernandez-Gonzalez, R. and Zallen, J. A. (2013). Wounded cells drive rapid epidermal repair in the early Drosophila embryo. *Mol. Biol. Cell* **24**, 3227-3237.

Fernandez-Gonzalez, R., de Matos Simoes, S., Röper, J.-C., Eaton, S. and Zallen, J. A. (2009). Myosin II dynamics are regulated by tension in intercalating cells. *Dev. Cell* **17**, 736-743.

Gaggioli, C., Hooper, S., Hidalgo-Carcedo, C., Grosse, R., Marshall, J. F., Harrington, K. and Sahai, E. (2007). Fibroblast-led collective invasion of carcinoma cells with differing roles for RhoGTPases in leading and following cells. *Nat. Cell Biol.* **9**, 1392-1400.

Glantz, S. A. (2002). *Primer of Biostatistics*. New York: McGraw-Hill, Medical Pub. Div.

Hayakawa, K., Tatsumi, H. and Sokabe, M. (2011). Actin filaments function as a tension sensor by tension-dependent binding of cofilin to the filament. *J. Cell Biol.* **195**, 721-727.

Heller, E., Kumar, K. V., Grill, S. W. and Fuchs, E. (2014). Forces generated by cell intercalation tow epidermal sheets in mammalian tissue morphogenesis. *Dev. Cell* **28**, 617-632.

Hidalgo-Carcedo, C., Hooper, S., Chaudhry, S. I., Williamson, P., Harrington, K., Leitinger, B. and Sahai, E. (2011). Collective cell migration requires suppression of actomyosin at cell-cell contacts mediated by DDR1 and the cell polarity regulators Par3 and Par6. *Nat. Cell Biol.* **13**, 49-58.

Higashida, C., Kiuchi, T., Akiba, Y., Mizuno, H., Maruoka, M., Narumiya, S., Mizuno, K. and Watanabe, N. (2013). F- and G-actin homeostasis regulates mechanosensitive actin nucleation by formins. *Nat. Cell Biol.* **15**, 395-405.

Huang, J., Zhou, W., Dong, W., Watson, A. M. and Hong, Y. (2009). From the cover: directed, efficient, and versatile modifications of the Drosophila genome by genomic engineering. *Proc. Natl. Acad. Sci. USA* **106**, 8284-8289.

Hundt, N., Steffen, W., Pathan-Chhatbar, S., Taft, M. H. and Manstein, D. J. (2016). Load-dependent modulation of non-muscle myosin-2A function by tropomyosin 4.2. *Sci. Rep.* **6**, 20554.

Hutson, M. S., Tokutake, Y., Chang, M. S., Bloor, J. W., Venakides, S., Kiehart, D. P. and Edwards, G. S. (2003). Forces for morphogenesis investigated with laser microsurgery and quantitative modeling. *Science* **300**, 145-149.

Jégou, A., Carlier, M.-F. and Romet-Lemonne, G. (2013). Formin mDia1 senses and generates mechanical forces on actin filaments. *Nat. Commun.* **4**, 1883.

Jordan, P. and Karess, R. (1997). Myosin light chain-activating phosphorylation sites are required for oogenesis in Drosophila. *J. Cell Biol.* **139**, 1805-1819.

Kasza, K. E., Farrell, D. L. and Zallen, J. A. (2014). Spatiotemporal control of epithelial remodeling by regulated myosin phosphorylation. *Proc. Natl. Acad. Sci. USA* **111**, 11732-11737.

Kiehart, D. P., Galbraith, C. G., Edwards, K. A., Rickoll, W. L. and Montague, R. A. (2000). Multiple forces contribute to cell sheet morphogenesis for dorsal closure in Drosophila. *J. Cell Biol.* **149**, 471-490.

Kofron, M., Heasman, J., Lang, S. A. and Wylie, C. C. (2002). Plakoglobin is required for maintenance of the cortical actin skeleton in early Xenopus embryos and for cdc42-mediated wound healing. *J. Cell Biol.* **158**, 695-708.

Komatsu, S., Yano, T., Shibata, M., Tuft, R. A. and Ikebe, M. (2000). Effects of the regulatory light chain phosphorylation of myosin II on mitosis and cytokinesis of mammalian cells. *J. Biol. Chem.* **275**, 34512-34520.

Kovacs, M., Thirumurugan, K., Knight, P. J. and Sellers, J. R. (2007). Load-dependent mechanism of nonmuscle myosin 2. *Proc. Natl. Acad. Sci. USA* **104**, 9994-9999.

Leung, C. Y. B. and Fernandez-Gonzalez, R. (2015). Quantitative image analysis of cell behavior and molecular dynamics during tissue morphogenesis. *Methods Mol. Biol.* **1189**, 99-113.

Lienkamp, S. S., Liu, K., Karner, C. M., Carroll, T. J., Ronneberger, O., Wallingford, J. B. and Walz, G. (2012). Vertebrate kidney tubules elongate using a planar cell polarity-dependent, rosette-based mechanism of convergent extension. *Nat. Genet.* **44**, 1382-1387.

Martin, P. and Lewis, J. (1992). Actin cables and epidermal movement in embryonic wound healing. *Nature* **360**, 179-183.

Nagy, A., Takagi, Y., Billington, N., Sun, S. A., Hong, D. K. T., Homsher, E., Wang, A. and Sellers, J. R. (2013). Kinetic characterization of nonmuscle myosin IIb at the single molecule level. *J. Biol. Chem.* **288**, 709-722.

Norstrom, M. F., Smithback, P. A. and Rock, R. S. (2010). Unconventional processive mechanics of non-muscle myosin IIB. *J. Biol. Chem.* **285**, 26326-26334.

Pines, M., Das, R., Ellis, S. J., Morin, A., Czerniecki, S., Yuan, L., Klose, M., Coombs, D. and Tanentzapf, G. (2012). Mechanical force regulates integrin turnover in Drosophila in vivo. *Nat. Cell Biol.* **14**, 935-943.

Pouille, P.-A., Ahmadi, P., Brunet, A.-C. and Farge, E. (2009). Mechanical signals trigger Myosin II redistribution and mesoderm invagination in Drosophila embryos. *Sci. Signal.* **2**, ra16.

Royou, A., Field, C., Sisson, J. C., Sullivan, W. and Karess, R. (2004). Reassessing the role and dynamics of nonmuscle myosin II during furrow formation in early Drosophila embryos. *Mol. Biol. Cell* **15**, 838-850.

Rozbicki, E., Chuai, M., Karjalainen, A. I., Song, F., Sang, H. M., Martin, R., Knölker, H.-J., MacDonald, M. P. and Weijer, C. J. (2015). Myosin-II-mediated cell shape changes and cell intercalation contribute to primitive streak formation. *Nat. Cell Biol.* **17**, 397-408.

Scholey, J. M., Taylor, K. A. and Kendrick-Jones, J. (1980). Regulation of non-muscle myosin assembly by calmodulin-dependent light chain kinase. *Nature* **287**, 233-235.

Sellers, J. R., Eisenberg, E. and Adelstein, R. S. (1982). The binding of smooth muscle heavy meromyosin to actin in the presence of ATP. Effect of phosphorylation. *J. Biol. Chem.* **257**, 13880-13883.

Sellers, J. R., Spudich, J. A. and Sheetz, M. P. (1985). Light chain phosphorylation regulates the movement of smooth muscle myosin on actin filaments. *J. Cell Biol.* **101**, 1897-1902.

Simone, R. P. and DiNardo, S. (2010). Actomyosin contractility and Discs large contribute to junctional conversion in guiding cell alignment within the Drosophila embryonic epithelium. *Development* **137**, 1385-1394.

Tojkander, S., Gateva, G., Husain, A., Krishnan, R. and Lappalainen, P. (2015). Generation of contractile actomyosin bundles depends on mechanosensitive actin filament assembly and disassembly. *Elife* **4**, e06126.

Vasquez, C. G., Tworoger, M. and Martin, A. C. (2014). Dynamic myosin phosphorylation regulates contractile pulses and tissue integrity during epithelial morphogenesis. *J. Cell Biol.* **206**, 435-450.

Vasquez, C. G., Heissler, S. M., Billington, N., Sellers, J. R. and Martin, A. C. (2016). Drosophila non-muscle myosin II motor activity determines the rate of tissue folding. *elife* **5**, pii: e20828.

Wood, W., Jacinto, A., Grose, R., Woolner, S., Gale, J., Wilson, C. and Martin, P. (2002). Wound healing recapitulates morphogenesis in Drosophila embryos. *Nat. Cell Biol.* **4**, 907-912.

Zulueta-Coarasa, T. and Fernandez-Gonzalez, R. (2015). Laser ablation to investigate cell and tissue mechanics *in vivo*. In *Integrative Mechanobiology: Micro- and Nano- Techniques in Cell Mechanobiology* (ed. Y. Sun, D. Kim and C. Simmons). Cambridge University Press, Cambridge, UK.

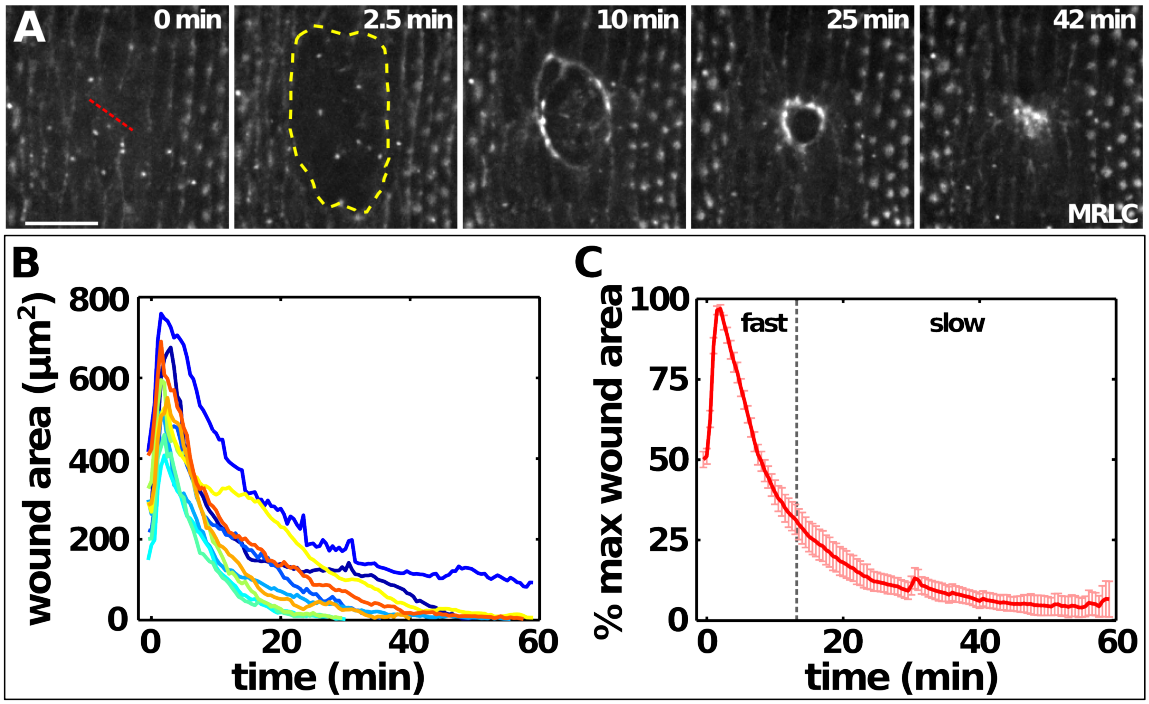

Figure S1. Embryonic wound repair occurs in a fast and a slow phase. (A) Wound closure in an embryo expressing MRLC:GFP. Red line indicates wound site. Yellow dashed line outlines the wound. Bar, 10 µm. Anterior left, ventral down. **(B)** Wound area over time. Each line represents a different wound and embryo. **(C)** Mean wound area over time (n=10 wounds) normalized to the maximum wound area. Different wounds reach their maximum area at slightly different times. Dashed line indicates the transition from fast to slow wound repair. **(A-C)** Time is with respect to wounding.

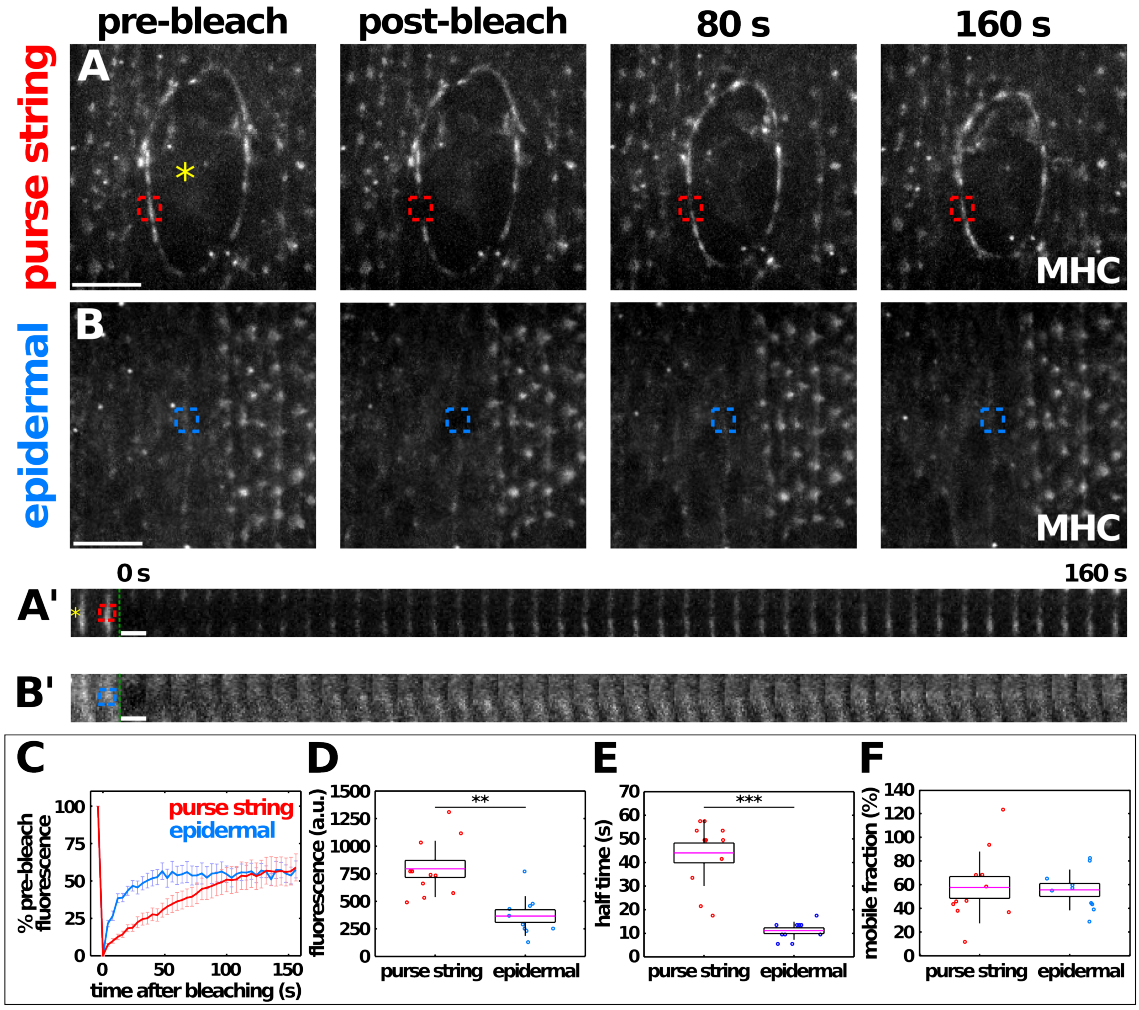

Figure S2. Reduced MHC turnover at the purse string. (A-B) FRAP experiments in wounded embryos expressing MHC:GFP. Regions were photobleached on the purse string (A, red) or an epidermal myosin cable (B, blue). Bars, 10 µm (A-B) and 4 s (A'-B'). Yellow asterisks indicate the position of the wound. Anterior left, ventral down. Green dashed lines display time of photobleaching. **(C-F)** Percent pre-bleach fluorescence over time in the photobleached region (C, error bars, SEM), initial fluorescence (D), $t_{1/2}$ (E) and mobile fraction (F) in the purse string (red, n=11) and in epidermal cables (blue, n=10).

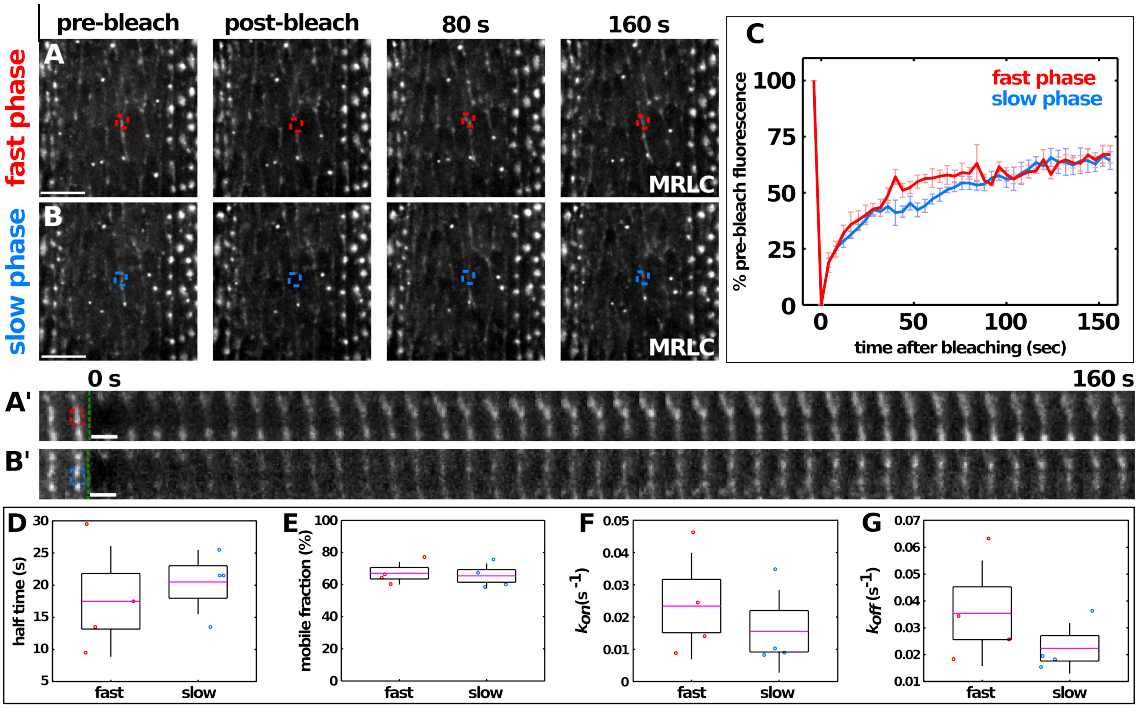

Figure S3. **Sequential photobleaching does not affect turnover measurements.** **(A-B)** FRAP experiments in wounded embryos expressing MRLC:GFP. Regions were sequentially photobleached on epidermal cables during the fast phase of wound closure (40-60% of the maximum wound area, A, red) or during the slow phase (≤ 10% of the maximum wound area, B, blue) of wound closure. Bars, 10 µm (A-B) and 4 s (A'-B'). Anterior left, ventral down. Green dashed lines display time of photobleaching. **(C-G)** Percent pre-bleach fluorescence over time in the photobleached region (C), $t_{1/2}$ (D), mobile fraction (E), k_{on} (F) and k_{off} (G) for the fast phase (red, $n = 4$) and the slow phase (blue, $n = 4$).

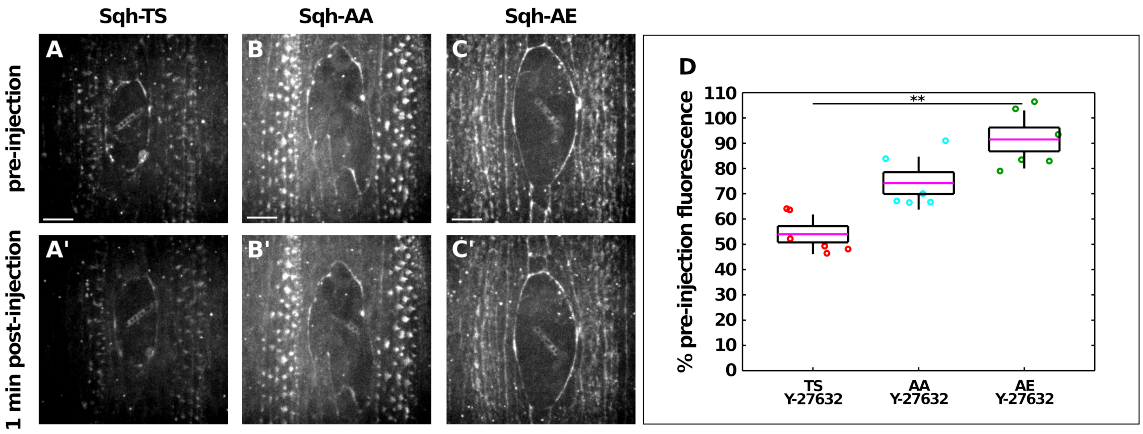

Figure S4. Y-27632 injection causes stronger localization phenotypes on wild-type than on phosphomutant myosin. (A-C) Time-lapse images before (A-C) or 1 min after (A'-C') injection of Y-27632 during wound repair in embryos expressing Sqh-TS, Sqh-AE, or Sqh-AA. Bars, 10 µm (A-C). Anterior left, ventral down. **(D)** Percent pre-injection fluorescence one minute after Y-27632 injection (Sqh-TS, *n*=6; Sqh-AA, *n*=6; Sqh-AE, *n*=6).

Movie S1. Myosin dynamics around wounds and in the intact epidermis. Epidermal cells expressing MRLC:GFP in a wounded (left) or intact (right) embryo. Images were acquired by time-lapse confocal microscopy using a spinning disk confocal microscope (Revolution XD; Andor Technology). A stack was acquired every 15 s for 34 min. Time is with respect to wounding. Anterior left, dorsal up.

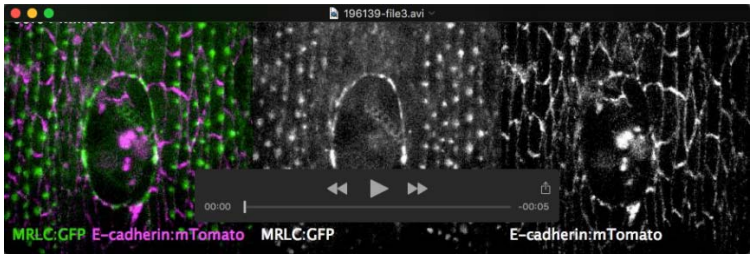

Movie S2. Measuring myosin turnover after purse string ablation. Epidermal cells expressing MRLC:GFP (left, green; centre) and E-cadherin:mTomato (left, magenta; right) in a wounded embryo. White arrowheads indicate photobleaching sites adjacent (top) or far (bottom) from the ablation site. Images were acquired by time-lapse confocal microscopy using a spinning disk confocal microscope (Revolution XD; Andor Technology). A stack was acquired every 4 s for 1 minute. Time is with respect to purse string ablation. Anterior left, dorsal up.

Movie S3. Myosin localization after Y-27632 injection. Wounded embryos expressing wild-type (Sqh-TS, left), unphosphorylatable (Sqh-AA, centre), or phosphomimetic (Sqh-AE, right) myosin. Images were acquired by time-lapse confocal microscopy using a spinning disk confocal microscope (Revolution XD; Andor Technology). A stack was acquired every 30 s for 3 minutes. Time is with respect to Y-27632 injection. Anterior left, dorsal up.